

CO emissions from optically selected galaxies at $z \sim 0.1 - 0.2$: Tight anti-correlation between molecular gas fraction and 4000 Å break strength

Kana MOROKUMA-MATSUI

Nobeyama Radio Observatory, 462-2 Nobeyama, Minamimaki-mura, Minamisaku-gun, Nagano 384-1305
kana.matsui@nao.ac.jp

Junichi BABA

Earth-Life Science Institute, Tokyo Institute of Technology, 2-12-1-IE-29 Ookayama, Meguro-ku, Tokyo, 152-8550
babajn@elsi.jp

Kazuo SORAI

Department of Physics/Department of CosmoSciences, Hokkaido University, Sapporo, Hokkaido 060-0810
sorai@astro1.sci.hokudai.ac.jp

and

Nario KUNO

Faculty of Pure and Applied Sciences, University of Tsukuba, 1-1-1, Tennoudai, Tsukuba, Ibaraki 350-8577
kuno.nario.gt@u.tsukuba.ac.jp

(Received ; accepted)

Abstract

We performed $^{12}\text{CO}(J=1-0)$ (hereafter, CO) observations towards 12 normal star-forming galaxies with stellar mass of $M_\star = 10^{10.6} - 10^{11.3} M_\odot$ at $z = 0.1 - 0.2$ with the 45-m telescope at the Nobeyama Radio Observatory (NRO). The samples are selected with $D_n(4000)$ that is a strength of the 4000 Å break, instead of commonly used far-infrared (FIR) flux. We successfully detect the CO emissions from eight galaxies with signal-to-noise ratio (S/N) larger than three, demonstrating the effectiveness of the $D_n(4000)$ -based sample selection. For the first time, we find a tight anti-correlation between $D_n(4000)$ and molecular gas fraction (f_{mol}) using literature data of nearby galaxies in which the galaxies with more fuel for star formation have younger stellar populations. We find that our CO-detected galaxies at $z \sim 0.1 - 0.2$ also follow the same relation of nearby galaxies. This implies that the galaxies evolve along this $D_n(4000) - f_{\text{mol}}$ relation, and that $D_n(4000)$ seems to be used as a proxy for f_{mol} which requires many time-consuming observations. Based on the comparison with the model calculation with a population synthesis code, we find that star formation from metal enriched gas and its quenching in the early time are necessary to reproduce galaxies with large $D_n(4000)$ and non-zero gas fraction.

Key words: Galaxies: evolution – Galaxies: ISM

1. Introduction

The redshift range of $z < 1$ is the key epoch for revealing formation and evolution of disk galaxies. Large surveys in the optical and near infrared (NIR) wavelengths have revealed important observational evidence for the dependence of galaxy evolution on its stellar mass: 1) the bimodal distribution in color with the boundary mass of $M_\star = 10^{10.5} M_\odot$ (e.g., Strateva et al. 2001; Kauffmann et al. 2003), 2) galaxies with $M_\star < 10^{10.5} M_\odot$ and $M_\star > 10^{10.5} M_\odot$ consist of the later- and earlier-type galaxies, respectively (e.g., Conselice 2006), 3) massive galaxies with $M_\star > 10^{11} M_\odot$ acquired most of their stellar mass before $z = 1$ while less massive galaxies with $M_\star < 10^{10} M_\odot$ acquired most of their stellar mass after $z = 1$ (e.g., Leitner 2012), 4) for Milky-Way size galaxies, only galactic disks have evolved in $z < 1$ and both bulges and disk have been formed by $z > 1$ (e.g., van Dokkum et al. 2013). These indicate that the redshift range of $z < 1$ is the growing pe-

riod for disk galaxies in terms of stellar mass. In addition, local disk galaxies have evolved their galactic disks in this epoch.

Understanding of the stellar component of galaxies at $z < 1$ has progressed but there is a very small number of studies on molecular gas of normal galaxies at the redshift range¹ (Geach et al. 2011; Matsui et al. 2012; Bauermeister et al. 2013). The next most abundant molecule, carbon monoxide (hereafter, CO) after H_2 has been widely utilized to measure molecular gas mass since the H_2 molecule does not radiate line emission in a cold environment such as molecular clouds whose typical tem-

¹ There are studies on Ultra Luminous InfraRed Galaxies (ULIRGs) in this redshift range (Solomon et al. 1997; Chung et al. 2009; Combes et al. 2013), showing that both the molecular gas fraction and star-formation efficiency play an important role in cosmic SFR evolution (Combes et al. 2013). However, most of them have signs of merging (e.g., close pair of galaxies and tidal features), thus they are not expected to be normal galaxies.

perature is a few tens Kelvin. One of the reasons for the small number of CO observations in $z < 1$ is the limitation from the atmospheric window. The so-called 3-mm window restricted by O_2 of atmosphere of the earth is opened around $\sim 80 - 115$ GHz, which constrains the redshift of $z < 0.44$ in the case of observations in $CO(J=1-0)$ whose rest-frame frequency is 115.271 GHz.

The sample selection with far infrared (FIR) flux also prevents the number of CO observations toward normal galaxies from increasing in $z < 1$. For the time-consuming CO observations, it is preferred to observe galaxies with the coordinate, spectroscopic redshift and expected intensity. Although the catalogue of a large optical survey contains the data of coordinate and redshift of many galaxies (e.g., $\sim 10^9$ for SDSS Date Release 9, Ahn et al. 2012), the number drastically decreases if the candidates are crossmatched with FIR catalogue. In addition, sample selection based on FIR flux obviously biases to IR bright objects such as Ultra Luminous InfraRed Galaxies (ULIRGs) whose IR luminosities are $L_{IR} > 10^{12}L_{\odot}$ (Sanders & Mirabel 1996). The majority of local ULIRGs are reported as mergers with tidal features (Sanders et al. 1988). Therefore, to select normal galaxies, sample selection based on FIR flux is not an optimal choice.

We performed $^{12}CO(J=1-0)$ (hereafter, CO) observations toward normal galaxies at $z \sim 0.1 - 0.2$ with the 45-m telescope at the Nobeyama Radio Observatory (NRO)² to fill the observational gap in $0.1 < z < 1.0$. For the sample selection, we use optical data instead of FIR data to increase the number of candidates and select normal galaxies rather than IR-bright galaxies.

The structure of this paper is as follows: The observational information and data reductions are described in section 2. The obtained CO spectra and the relations between molecular gas fraction and optical indices are shown in section 3. We investigate the relation between the star-formation history and gas fraction with model calculation in section 4. Finally, we summarize this work in section 5. We adopt $H_0 = 71 \text{ km s}^{-1}$, $\Omega_M = 0.27$ and $\Omega_{\Lambda} = 0.73$.

2. Observations

2.1. Sample Selection

Sample galaxies are selected using SDSS DR9 (Ahn et al. 2012), which contains the photometric or spectroscopic data of $\sim 10^9$ objects³. The basic criteria for the sample selection are as follows: 1) $-20 < \text{Dec.} < +30$ degree, 2) $0.1 < z < 0.23$, 3) apparent size: Petrosian radius > 4 arcsec, 4) nuclear activity: HII, 5) morphology: disk galaxy, 6) $D_n(4000) < 1.4$.

The declination range is determined so that the objects are observable with ALMA as well as with the 45-m telescope at NRO for a further investigation of gas distribution and kinematics, which are important for understand-

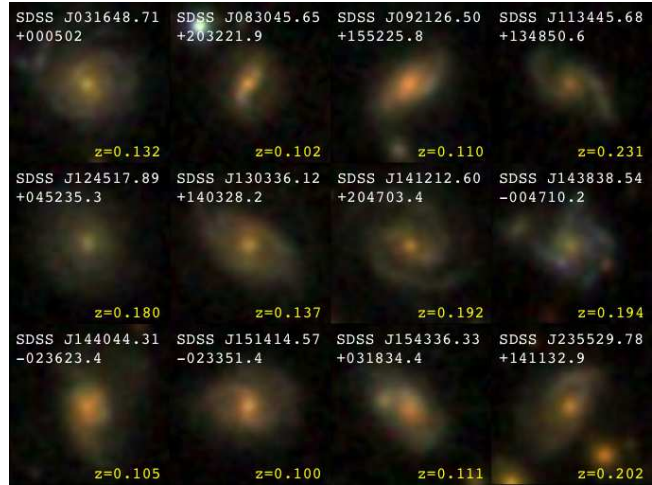


Fig. 1. SDSS optical three-color images of the sample galaxies. The image size is $20'' \times 20''$.

ing the detailed physical properties of gas component in galaxies. We put the criterion of apparent disk size to check the morphology of disk galaxy (higher likelihood in fitting of galaxy light profile with exponential than de Vaucouleurs, Strateva et al. 2001). Active galactic nuclei (AGN) are excluded from our samples using a set of nebular emission line diagrams (Baldwin, Phillips & Terlevich, “BPT” diagram, Baldwin et al. 1981) to reduce the contamination of light from AGN and estimate star-formation rate (SFR) accurately.

We did not use FIR fluxes but $D_n(4000)$ to select sample galaxies. $D_n(4000)$ is a measure of the strength of 4000 Å break and is defined as

$$D_n(4000) = \frac{(\lambda_2^- - \lambda_1^-) \int_{\lambda_1^+}^{\lambda_2^+} F_\nu d\lambda}{(\lambda_2^+ - \lambda_1^+) \int_{\lambda_1^-}^{\lambda_2^-} F_\nu d\lambda}, \quad (1)$$

where $(\lambda_1^-, \lambda_2^-, \lambda_1^+, \lambda_2^+) = (3850, 3950, 4000, 4100)$ in Å (Balogh et al. 1999). This value allows us to constrain the mean stellar age of a galaxy where lower $D_n(4000)$ indicates younger stellar population and vice versa (Kauffmann et al. 2003). If we consider single-burst populations, the 4000 Å break, which is characteristic of cooler stars with types later than about G0, becomes dominant at older ages. This is due to the sudden onset of absorption features bluewards 4000 Å produced notably by Ca II H and K, Fe I, Mg I, and CN lines. Kauffmann et al. (2012) showed that CO-detected galaxies in the COLD GASS project (Saintonge et al. 2011) have lower value of $D_n(4000)$ (< 1.4). We use this empirical criteria for the sample selection instead of commonly used FIR flux. The SDSS images of the sample galaxies are shown in figure 1.

2.2. Observations with the 45-m telescope at NRO

We observed 12 disk galaxies at $z \sim 0.1 - 0.2$ in the CO ($J=1-0$) line during the observing periods of 2012/2013 and 2013/2014 winter seasons in Japan. The line frequency was shifted to between 93.638 GHz and 104.749 GHz from the rest frequency of 115.271 GHz according to

² Nobeyama Radio Observatory is a branch of the National Astronomical Observatory of Japan, National Institutes of Natural Sciences.

³ <http://skyserver.sdss3.org/dr9/en/>

the redshifts of the sample galaxies. We used a new two-beam, two-polarization, sideband separating SIS receiver, TZ (Two-beam sideband-separating SIS receiver for Z-machine) (Nakajima et al. 2013) and SAM45 (Spectral Analysis Machine for the 45-m telescope) which is a copy of a part of the FX-type correlator for the Atacama Compact Array (ACA). The image rejection ratios (IRRs) of TZ were measured at each observing frequency in every observation. The values of IRRs were 8–20 dB at the center of the intermediate frequency (IF) through the observations. The system noise temperature, T_{sys} , was typically 150–240 K during our observations. Telescope pointing was checked every 50 minutes through observing SiO maser sources close to our target galaxies at 43 GHz. We used the data that were observed with pointing accuracy better than 5 arcsec. The main beam size, θ_{B} is ~ 18 arcsec around 100 GHz, which corresponds to ~ 31 kpc at the lowest redshift of sample galaxies ($z = 0.10$), and to ~ 66 kpc at the highest ($z = 0.23$). All data were calibrated by the standard chopper wheel method, and converted from antenna temperature T_a^* scale into main-beam brightness temperature by $T_{\text{mb}} = T_a^* / \eta_{\text{mb}}$. The main beam efficiencies, η_{mb} in the 2012/2013 and 2013/2014 seasons at the observing frequencies were 0.33–0.35 and 0.37–0.41, respectively.

2.3. Data reduction

Data reduction is performed using the NEWSTAR software, which was developed by NRO based on the Astronomical Image Processing System (AIPS) package. Integration time of each galaxy is typically six hours summed up for the both polarizations, and the typical r.m.s. noise temperature was in the range of 1–8 mK in T_{mb} scale after binning up to 40 km s $^{-1}$ resolution. Integrated intensity, I_{CO} , is calculated according to $I_{\text{CO}} = \int T_{\text{mb}} dv$. The error of I_{CO} , ΔI_{CO} , is estimated as $T_{\text{r.m.s.}} \sqrt{\Delta V_e \Delta v}$, where $T_{\text{r.m.s.}}$ is the r.m.s. noise temperatures at velocity resolution of Δv , which is the velocity resolution of final spectrum. ΔV_e is the full line width within which the integrated intensity is calculated. In the case where the peak temperature of the emission line has a signal-to-noise ratio (S/N) less than three, the upper limit of 3 ΔI_{CO} was adopted as I_{CO} .

CO line luminosity, L'_{CO} is calculated from the integrated intensity and beam solid angle $\Omega_{\text{b}} = \pi \theta_{\text{B}}^2 / 4 \ln 2$ (θ_{B} in radians) as

$$L'_{\text{CO}} = \frac{\Omega_{\text{b}} I_{\text{CO}} D_L^2}{(1+z)^3} \quad (\text{K km s}^{-1} \text{ pc}^2), \quad (2)$$

where D_L is a luminosity distance.

Molecular gas mass, M_{mol} , is calculated with L'_{CO} and a CO-to-H $_2$ conversion factor, α_{CO} as $M_{\text{mol}} = 1.36 \alpha_{\text{CO}} L'_{\text{CO}}$, where 1.36 is a factor to account for the contribution of He by mass. We adopt the typical Galactic value of $\alpha_{\text{CO}} = 4.3 M_{\odot} (\text{K km s}^{-1} \text{ pc}^2)^{-1}$ (corresponding to $X_{\text{CO}} = 2 \times 10^{20} \text{ cm}^{-2} [\text{K km s}^{-1}]^{-1}$), which is widely used for star-forming galaxies in the high- z universe (Tacconi et al. 2013) as well as local normal galaxies (Bolatto et al. 2013).

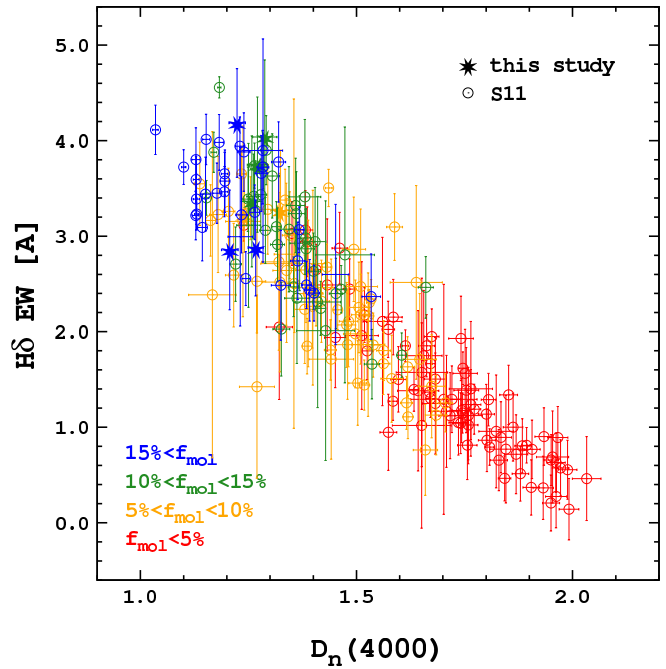


Fig. 5. Correlation between $D_n(4000)$ and $H\delta$ EW. Observed galaxies at $z \sim 0.1 - 0.2$ and local galaxies (COLD GASS, Saintonge et al. 2011) are shown as filled and open circles. The color is determined according to f_{mol} in which $f_{\text{mol}} > 15\%$ as blue, $10 < f_{\text{mol}} < 15\%$ as green, $5 < f_{\text{mol}} < 10\%$ as orange and $f_{\text{mol}} < 5\%$ as red.

3. Results

3.1. CO spectra

Figure 2 shows the obtained CO spectra binned with a velocity resolution of 40 km s $^{-1}$. We successfully detect CO emission from six galaxies with S/N (peak temperature) larger than four, and tentatively from two galaxies ($3 \leq \text{S/N} < 4$) while the remaining four galaxies do not show significant CO emission ($\text{S/N} < 3$). This high detection rate (67 %) indicates the effectiveness of the sample selection based on $D_n(4000)$. The fitting result with a Gaussian is also plotted with blue solid line for the emission lines with $\text{S/N} \geq 3$. I_{CO} , full width at half maximum (FWHM), molecular gas mass (M_{mol}) and molecular gas fraction (f_{mol} , equation (3)) are presented in table 1. I_{CO} is calculated by summing the intensity within the velocity range colored in red in figure 2. FWHM in this table is estimated with a Gaussian fitting. Although the line profiles of the galactic CO spectra are not well described by a Gaussian as in figure 2, we here present the FWHM for reference, which are not used in the following analysis.

3.2. Star-formation history

An optical spectrum of a galaxy is the sum of the continuum and absorption spectra of stellar components and nebular emissions from ionized gas. In addition, stellar spectrum is different according to the stellar type. Stellar types that dominate the galactic optical light change with time and then the characteristic spectral features accordingly change with time (e.g., Fioc & Rocca-Volmerange

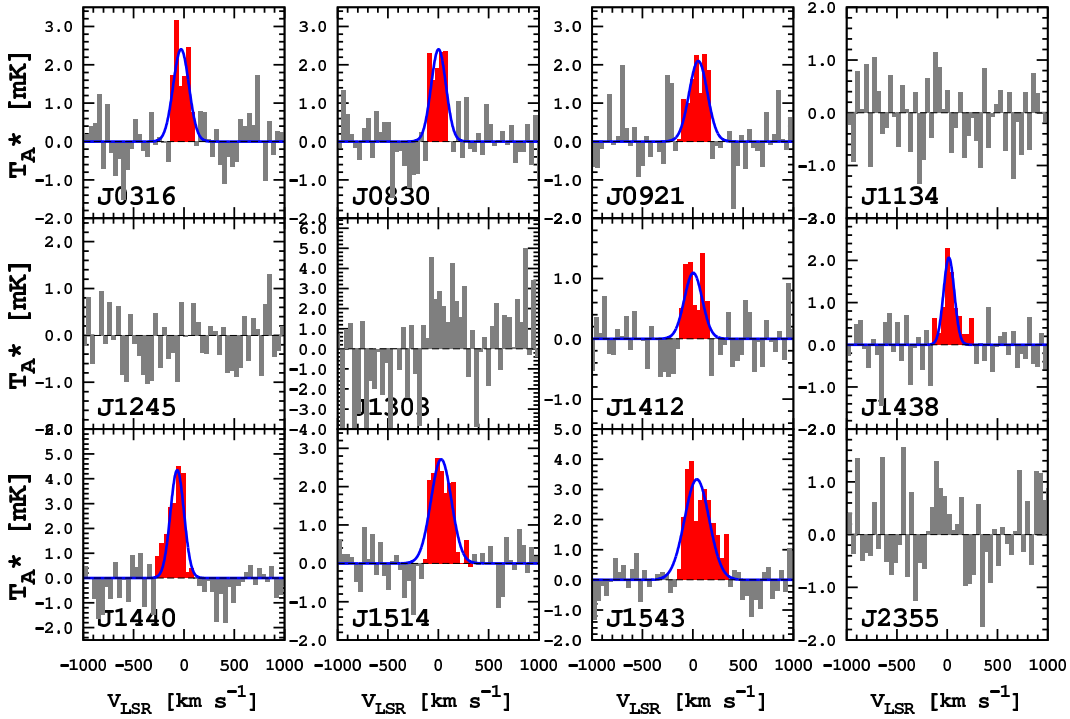


Fig. 2. CO spectra obtained with the 45-m telescope at NRO. The unit of the vertical axis is antenna temperature T_A^* and the velocity resolution is 40 km s^{-1} . I_{CO} is calculated by summing the intensity within the velocity range colored in red. The fitting results with a Gaussian are also shown in blue lines in case of $S/N \geq 3$.

Table 1. General information and observed results of the sample galaxies.

SDSS Name	z	M_\star^* $\log(M_\star/M_\odot)$	SFR* (M_\odot/yr)	$D_n(4000)^*$	I_{CO} (K km s^{-1})	FWHM (km s^{-1})	M_{mol} $(10^9 M_\odot)$	f_{mol} $(\%)$
J031648.71+000502.5	0.1315	10.79	10.8	1.27 ± 0.02	1.35 ± 0.18	185 ± 53	11.8 ± 1.5	16.1 ± 1.8
J083045.65+203221.9	0.1021	10.55	16.1	1.27 ± 0.02	1.14 ± 0.14	174 ± 50	6.03 ± 0.77	14.6 ± 1.6
J092126.50+155225.8	0.1097	10.94	18.7	1.24 ± 0.01	1.37 ± 0.24	214 ± 53	8.32 ± 1.47	8.7 ± 1.4
J113445.68+134850.6	0.2310	10.88	21.8	1.25 ± 0.03	< 0.48	—	< 12.8	< 14.4
J124517.89+045235.3	0.1800	10.75	19.0	1.23 ± 0.03	< 0.67	—	< 10.9	< 16.2
J130336.12+140328.2	0.1369	10.92	8.47	$1.45 \pm 0.03^{**}$	< 2.46	—	< 23.3	< 21.7
J141212.60+204703.4	0.1925	11.09	18.0	1.32 ± 0.02	0.73 ± 0.12	209 ± 89	13.5 ± 2.3	9.9 ± 1.5
J143838.54-004710.2	0.1940	10.62	13.4	1.21 ± 0.02	0.76 ± 0.16	127 ± 30	14.4 ± 3.0	25.8 ± 4.0
J144044.31-023623.4	0.1050	10.89	18.9	1.29 ± 0.03	2.45 ± 0.29	159 ± 28	9.18 ± 1.10	10.7 ± 1.1
J151414.57-023351.4	0.1005	10.73	11.0	1.26 ± 0.02	1.75 ± 0.16	240 ± 46	8.93 ± 0.82	14.3 ± 1.1
J154336.33+031834.4	0.1109	10.66	21.0	1.22 ± 0.02	3.28 ± 0.25	287 ± 84	20.4 ± 1.6	30.8 ± 1.6
J235529.78+141132.9	0.2015	11.31	48.4	1.34 ± 0.03	< 0.76	—	< 15.4	< 7.0

* M_\star , SFR and $D_n(4000)$ are retrieved from SDSS SkyServer DR10 (<http://skyserver.sdss3.org/dr10/en/>). M_\star is estimated from z -band magnitude to characterize the galaxy luminosity and M/L ratio from spectral indices of $D_n(4000)$ and $H\delta$ (Kauffmann et al. 2003; Tremonti et al. 2004). SFR is estimated from the attenuation-corrected $H\alpha$ luminosity (Brinchmann et al. 2004). The infrared luminosity (L_{IR}) inferred from SFR ranges $(5.67 - 32.1) \times 10^{10} L_\odot$ using $\log \text{SFR}(M_\odot \text{yr}^{-1}) = \log L_{\text{IR}}(\text{erg s}^{-1}) - 43.41$ (equation 12 of Kennicutt & Evans 2012), confirming that they are not ULIRGs.

** $D_n(4000)$ of this galaxies was listed as 1.30 ± 0.02 in DR9 but was changed to 1.45 ± 0.03 in DR10.

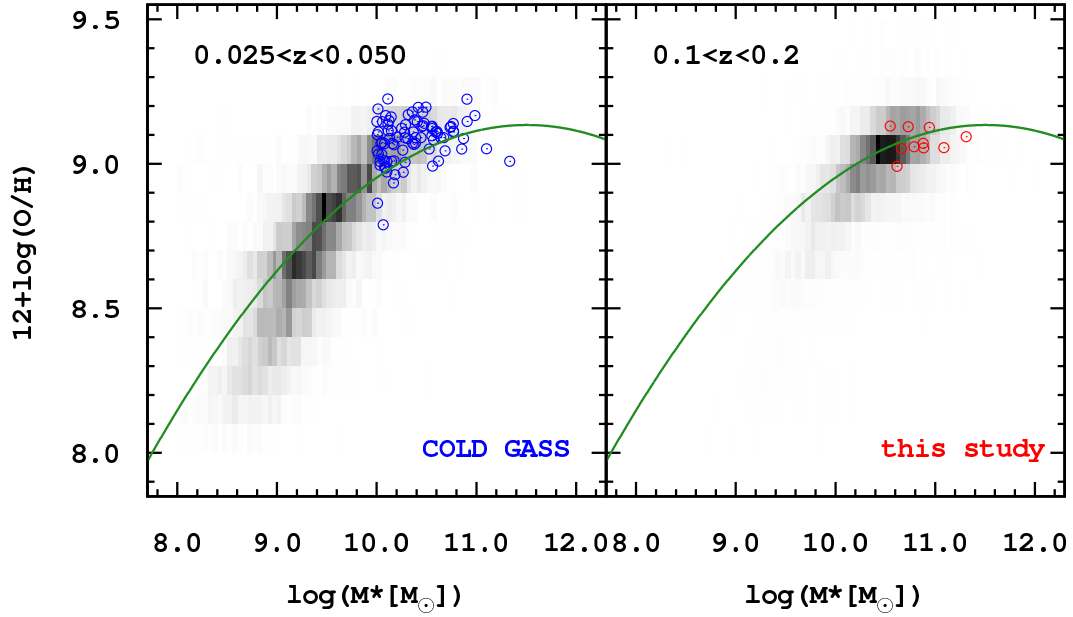


Fig. 3. Mass-metallicity relation of COLD GASS samples (Saintonge et al. 2011, blue open circles) and our observed galaxies at $z \sim 0.1 - 0.2$ (red open circles). An empirical mass-metallicity relation of local galaxies obtained in Tremonti et al. (2004) is shown as green solid line, as $12 + \log(\text{O}/\text{H}) = -1.492 + 1.847(\log M_*/M_\odot) - 0.08026(\log M_*/M_\odot)^2$. The background grey scale shows the distribution of 42,532 and 51,157 galaxies at $0.025 < z < 0.050$ and in $0.1 < z < 0.2$ as a reference.

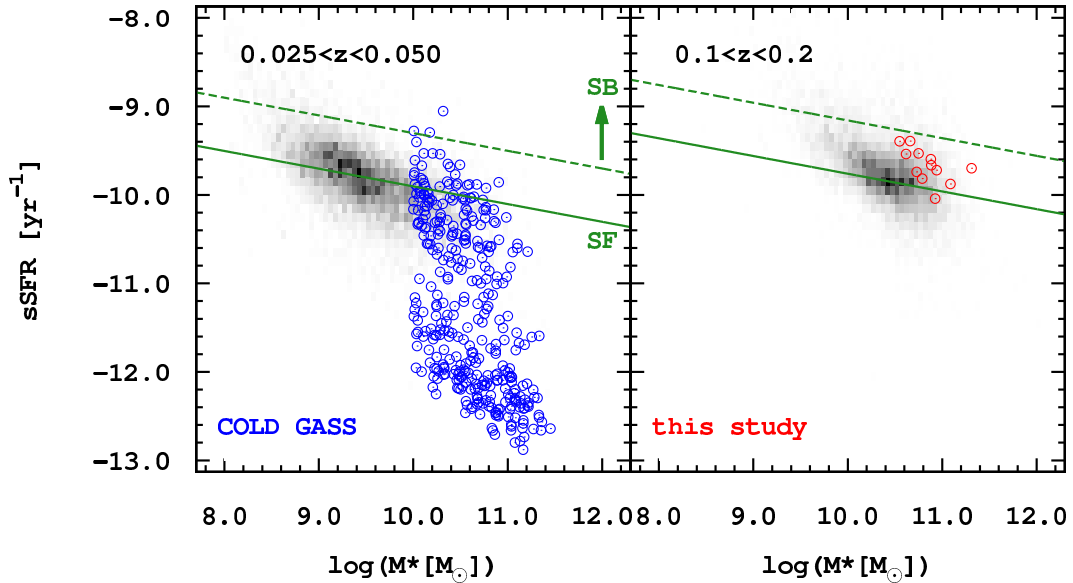


Fig. 4. Mass-sSFR relation of COLD GASS samples (Saintonge et al. 2011, blue open circles) and our observed galaxies at $z \sim 0.1 - 0.2$ (red open circles). An empirical mass-sSFR relation of star-forming galaxies obtained in Bauermeister et al. (2013) is shown as green solid line, as $\text{sSFR}_{\text{SF}} (\text{Gyr}^{-1}) = 0.07(1+z)^{3.2} \left(\frac{M_*}{10^{11} M_\odot}\right)^{-0.2}$. The green dashed line represents boundary between star-forming galaxies and starburst galaxies ($\text{sSFR}_{\text{SB}} > 4 \times \text{sSFR}_{\text{SF}}$). The background grey scale shows the distribution of 42,532 and 51,157 galaxies at $0.025 < z < 0.050$ and in $0.1 < z < 0.2$ as a reference.

1997; Bruzual & Charlot 2003). Therefore, previous studies have investigated the mean stellar ages and star-formation history of galaxies with those characteristic spectral features.

A tight anti-correlation between $D_n(4000)$ and $H\delta$ absorption has been studied to investigate the mean stellar age and star-formation history of galaxies (e.g., Balogh et al. 1999; Kauffmann et al. 2003). Measuring the strength of hydrogen Balmer lines in the galactic spectrum is one of the standard methods to derive luminosity-weighted mean ages from the integrated light of galaxies. Once O- and B-type stars have completed their evolution, Balmer lines become most outstanding in A-type star and weaken as a stellar population gets older. Kauffmann et al. (2003) investigated the mean stellar age and star-formation history statistically using SDSS data combined with the model calculations. They showed that $D_n(4000)$ constrains the mean stellar age of galaxies as described above and that the Balmer absorption-line index, $H\delta_A$ can constrain the fractional stellar mass formed in starburst events over the past few Gyr.

We retrieved catalogued data of $D_n(4000)$, $H\delta$ equivalent width (EW), stellar mass (M_*), SFR and metallicity ($12 + \log(O/H)$) of nearby galaxies and our observed galaxies from the SDSS DR10 (Ahn et al. 2014; Brinchmann et al. 2004; Tremonti et al. 2004). $H\delta$ EW is used as a measure of the strength of $H\delta$ absorption, where a larger $H\delta$ EW indicates a stronger absorption. The data of nearby galaxies is retrieved from COLD GASS (Saintonge et al. 2011), which is the largest unbiased CO survey toward nearby galaxies ($0.025 < z < 0.05$). Mass-metallicity and mass-specific SFR ($sSFR = SFR/M_*$) relations for these samples are shown in figures 3 and 4, respectively. Reference data are also plotted in grey scales, which are selected based on the redshift criteria, $0.025 < z < 0.050$ for COLD GASS sample and $0.1 < z < 0.2$ for our observed galaxies, and the criteria that their stellar mass, SFR and metallicity are properly calculated (i.e., not -999). In total, 42,532 and 51,157 galaxies were left as the reference samples. The green solid lines in figures 3 and 4 are empirical relations presented in Tremonti et al. (2004) and Bauermeister et al. (2013), respectively. The green dashed line in figure 4 represents the boundary between star-forming galaxies and starburst galaxies. In figure 3, COLD GASS samples and our observed galaxies are found in the plateau at high mass range of the mass-metallicity relation. Therefore, the variety in metallicity among these galaxies is expected to be small. In figure 4, our observed galaxies are all star-forming galaxies whereas COLD GASS samples include quenched galaxies as well.

In figure 5, we compare $D_n(4000)$ and $H\delta$ EW of our sample galaxies at $z \sim 0.1 - 0.2$ (filled star) with those of COLD GASS galaxies (open circle), confirming the anti-correlation reported in previous studies (Kauffmann et al. 2003). Moreover, the COLD GASS galaxies are distributed in a sufficiently wide range of $D_n(4000)$ for investigation of various star-formation histories of galaxies.

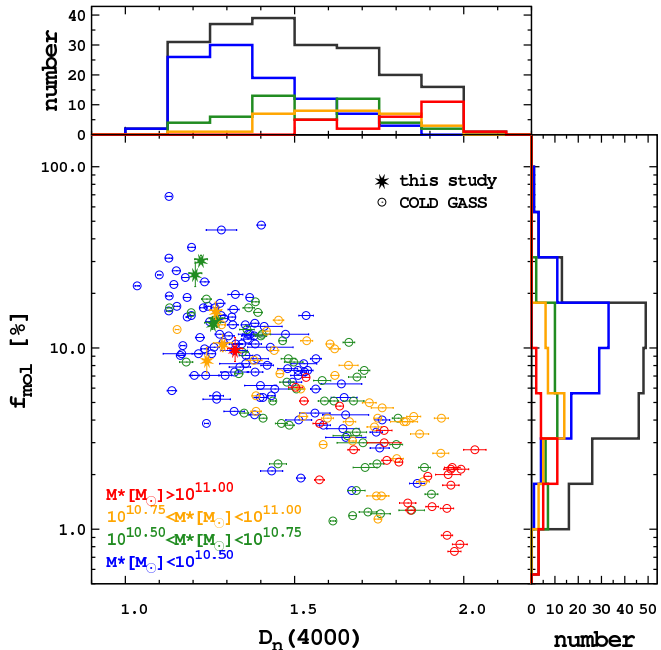


Fig. 6. Correlation between $D_n(4000)$ and f_{mol} . The symbols are the same as figure 5 but the color is determined according to stellar mass in which $M_*[M_\odot] > 10^{11}$ as red, $10^{10.75} < M_*[M_\odot] < 10^{11}$ as orange, $10^{10.50} < M_*[M_\odot] < 10^{10.75}$ as green and $M_*[M_\odot] < 10^{10.5}$ as blue.

3.3. Molecular gas fraction

In figure 5, we change the colors of the symbols according to their molecular gas fractions, $f_{\text{mol}} < 5\%$ as red, $5\% < f_{\text{mol}} < 10\%$ as orange, $10\% < f_{\text{mol}} < 15\%$ as green and $f_{\text{mol}} > 15\%$ as blue. Here, molecular gas fraction is defined as,

$$f_{\text{mol}}(\%) = \frac{M_{\text{mol}}}{M_{\text{mol}} + M_*} \times 100. \quad (3)$$

It is clearly seen that the COLD GASS galaxies with higher $H\delta$ EW and lower $D_n(4000)$ have higher gas fraction. In other words, more gas-rich galaxies have younger stellar components compared to the gas-poor galaxies. Our sample galaxies at $z \sim 0.1 - 0.2$ seem to follow the same $D_n(4000) - H\delta$ EW - f_{mol} relation. This clear trend indicates the existence of the relation between $D_n(4000)$ and f_{mol} .

Figure 6 shows the relation between $D_n(4000)$ and f_{mol} of our samples with CO detection ($S/N > 3$) and the COLD GASS galaxies. The symbols are the same as figure 5. As expected, a tight anti-correlation between $D_n(4000)$ and f_{mol} is seen in this figure, suggesting that $D_n(4000)$ could be used as a proxy for f_{mol} , which requires much telescope time to be measured. Since $D_n(4000)$ is calculated as a ratio of fluxes with 100 \AA widths, $D_n(4000)$ is easily measured compared to the normal spectral line indices such as $H\delta$ EW that require higher spectral resolution and S/N of each spectral channel than $D_n(4000)$. Therefore, $D_n(4000)$ might be a powerful tool to investigate molecular gas fraction of high- z galaxies (see also

Tacconi et al. 2013).

We checked the effect of the difference in the apparent size of galaxies on the $D_n(4000) - f_{\text{mol}}$ relation. $D_n(4000)$ is calculated with data taken within the 3-arcsec fiber in SDSS. The observed region is different according to the apparent galactic sizes. Therefore, we compare the apparent size of galaxies and $D_n(4000)$ of the COLD GASS sample. Even though there is no tight correlation between the apparent size of galaxy and $D_n(4000)$ (correlation factor of 0.07), galaxies larger than 18 arcsec and smaller than 6 arcsec seem to have higher and lower $D_n(4000)$, respectively. We exclude these larger and smaller samples but confirm the same trend seen in figure 6. Hence we conclude that the tight anti-correlation between $D_n(4000)$ and f_{mol} is not affected by the difference in the apparent galactic sizes.

The color of the symbols in figure 6 are determined according to the stellar mass. The anti-correlation between $D_n(4000)$ and f_{mol} is still seen even if we divide galaxies into four categories according to their stellar masses. Kauffmann et al. (2003) reported a bimodal distribution in stellar mass (M_*) – $D_n(4000)$ plot of galaxies, the first peak is found at $D_n(4000) \sim 1.3$ and the second peak at $D_n(4000) \sim 1.85$. They also showed that transition mass range ($10^{10} - 10^{11} M_\odot$) has a large dispersion in $D_n(4000)$. Our result suggests that the large dispersion of $D_n(4000)$ seen in $M_* - D_n(4000)$ is due to the difference in the molecular gas fraction, i.e., the amount of the fuel for the future star formation. It is notable that this result also indicates the stellar mass-dependent star-formation history is attributed to the difference in the amount of molecular gas in galaxies. The stellar mass dependence of f_{mol} evolution will be investigated in our forthcoming paper (Morokum-Matsui et al. in prep.).

Figure 7 shows the variations of (a) gas phase metallicity $12 + \log(\text{O}/\text{H})$, (b) sSFR, and (c) concentration parameter in the $D_n(4000) - f_{\text{mol}}$ plot. The concentration parameter, C is defined as the ratio of $C = R90/R50$, where $R90$ and $R50$ are the radii enclosing 90 % and 50 % of the Petrosian r -band luminosity (Petrosian 1976) of galaxies (Shimasaku et al. 2001). C is strongly related with Hubble type where early- and late-type galaxies have $C \geq 2.6$ and $C < 2.6$, respectively (Strateva et al. 2001). In figure 7a, we can see that $12 + \log(\text{O}/\text{H})$ was successfully measured only in star-forming galaxies whose optical spectra contain strong nebular emissions that are used to calculate $12 + \log(\text{O}/\text{H})$. However, the metallicity variation is expected to be small among COLD GASS and our samples, taking into account that these sample galaxies have stellar mass with $> 10^{10} M_\odot$ and that the plateau of mass-metallicity relation is located in $> 10^{10} M_\odot$ as well. We can see the anti-correlation between sSFR and $D_n(4000)$ in figure 7b, which was already reported in Brinchmann et al. (2004). Considering that sSFR is a measure of the current versus past star formation, the relation between sSFR and $D_n(4000)$ is not surprising. f_{mol} is related to sSFR as $f_{\text{mol}} = \frac{1}{1 + (t_{\text{dep}} \text{sSFR})^{-1}}$ (e.g., Tacconi et al. 2013), where t_{dep} is depletion timescale of molecular gas

by star formation ($= \frac{M_{\text{mol}}}{\text{sSFR}}$). If t_{dep} can be assumed to be constant, f_{mol} is a function of sSFR. Therefore the anti-correlation between $D_n(4000)$ and f_{mol} is also logical conclusion. Figure 7c shows the morphological dependence on $D_n(4000) - f_{\text{mol}}$ relation where late-type galaxies tend to have smaller $D_n(4000)$ and larger f_{mol} .

4. Discussion

4.1. Comparison with model predictions

In this section, we compare the observed $D_n(4000) - f_{\text{gas}}$ relationship and the evolutionary path in this parameter space predicted by a population synthesis code, PEGASE.2 (Fioc & Rocca-Volmerange 1997, hereafter PEGASE). PEGASE allows us to calculate chemical and mass evolution (both gas and stellar components) of galaxies consistently. We calculated the evolution of nine different types of galaxy (starburst: Burst; early-type galaxies: E, S0; spiral galaxies: Sa, Sb, Sbc, Sc, Sd; irregular galaxies: Im) according to template evolutionary scenarios for them (Fioc & Rocca-Volmerange 1997; Fioc & Rocca-Volmerange 1999; Le Borgne & Rocca-Volmerange 2002; Tsalmantza et al. 2007). In Fioc & Rocca-Volmerange (1999), the observed spectral energy distributions (SED, from optical to NIR) of ~ 800 nearby galaxies were used to compute the template SEDs for eight different morphological types (E, S0, Sa, Sb, Sbc, Sc, Sd, Im). SFRs for the eight types were assumed to be proportional to gas mass as $\text{SFR}(t) = \frac{1}{p2} M_{\text{gas}}(t)^{p1}$. In addition, SFR of starburst galaxies was modeled to be instantaneous, i.e., $\delta(t)$ (Tsalmantza et al. 2007). Exponential gas infall and galactic outflow are also considered. Galactic outflow is modeled to blow out all the existing gas in a galaxy at the specified time. Rana & Basu (1992) are adopted as the initial mass function (IMF). In this IMF, the slope in massive star range ($> 6 M_\odot$) is ~ -1.7 that is steeper than Salpeter IMF (-1.35 , Salpeter 1955). The parameters used for the calculation are summarized in tables 2 and 3.

PEGASE does not calculate evolution of molecular gas but total gas. Therefore we only use COLD GASS samples combined with available HI data (Cantinella et al. 2010), since our observed galaxies at $z \sim 0.1 - 0.2$ do not have HI data. The total gas fraction is calculated as

$$f_{\text{gas}}(\%) = \frac{M_{\text{HI}} + M_{\text{H}_2}}{M_{\text{HI}} + M_{\text{H}_2} + M_*} \times 100. \quad (4)$$

Figure 8a shows the comparison between the observed $D_n(4000) - f_{\text{gas}}$ and the results of model calculations for each galaxy type. Even though the dispersion of the relation is enlarged, there is the same trend in the $D_n(4000) - f_{\text{gas}}$ relation of COLD GASS samples, such as one found in figure 6 where galaxies with higher gas fraction have lower $D_n(4000)$. We can see that the template models reproduce the observed trend where gas-rich galaxies tend to have lower $D_n(4000)$ in figure 8a. In addition, it is also reproduced that the later-type galaxies tend to be distributed in the upper left in this plot (see figure 7c). This qualitative consistency roughly supports the differ-

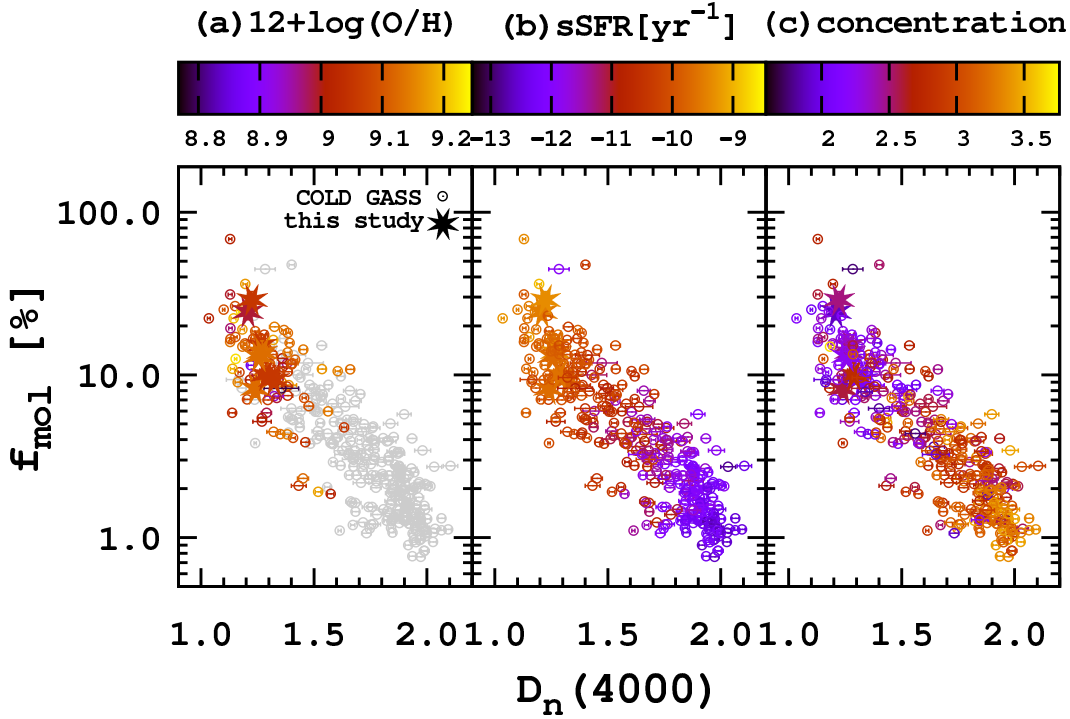


Fig. 7. Same as figure 6 but with color coding for (a) gas phase metallicity ($12 + \log(\text{O}/\text{H})$), (b) specific SFR ($\text{sSFR} = \text{SFR}/M_*$) and (c) concentration parameter ($C = R90/R50$). Galaxies without metallicity measurement are shown as grey symbols in (a).

Table 2. Common parameters for all template galaxies in PEGASE.2 (Fioc & Rocca-Volmerange 1997).

Parameters	Values
SNII ejecta of massive stars	model B of Woosley & Weaver (1995)
Stellar winds	yes
Initial mass function	Rana & Basu (1992)
Lower mass	$0.09 M_{\odot}$
Upper mass	$120 M_{\odot}$
Fraction of close binary systems	0.05
Initial metallicity	0.00
Metallicity of the in falling gas	0.00
Consistent evolution of the stellar metallicity	yes
Mass fraction of substellar objects	0.00
Nebular emission	yes

Table 3. PEGASE.2 parameters* for each template galaxy.

Type	p1	p2	infall	galactic winds	extinction	age
		[Myr/ M_{\odot}]	[Myr]	[Gyr]		[Gyr]
Burst	–	–	–	–	inclination-averaged disk geometry	2
E	1	300	300	1	spheroidal geometry	13
S0	1	500	100	5	spheroidal geometry	13
Sa	1	1408.5	2800	–	inclination-averaged disk geometry	13
Sb	1	2500	3500	–	inclination-averaged disk geometry	13
Sbc	1	5714.3	6000	–	inclination-averaged disk geometry	13
Sc	1	10000	8000	–	inclination-averaged disk geometry	13
Sd	1	14286	8000	–	inclination-averaged disk geometry	13
Im	1.5	15385	8000	–	inclination-averaged disk geometry	9

* Burst model assumes $\delta(t)$ for star-formation history and the other models assume SFR as $SFR(t) = \frac{1}{p_2} M_{\text{gas}}(t)^{p_1}$. “infall” represents the starting time of the gas accretion in Myr. If there are numbers in the “galactic winds” column, the mass of gas in the galaxy becomes zero at the time. “age” corresponds to the age of the galaxy at $z = 0$.

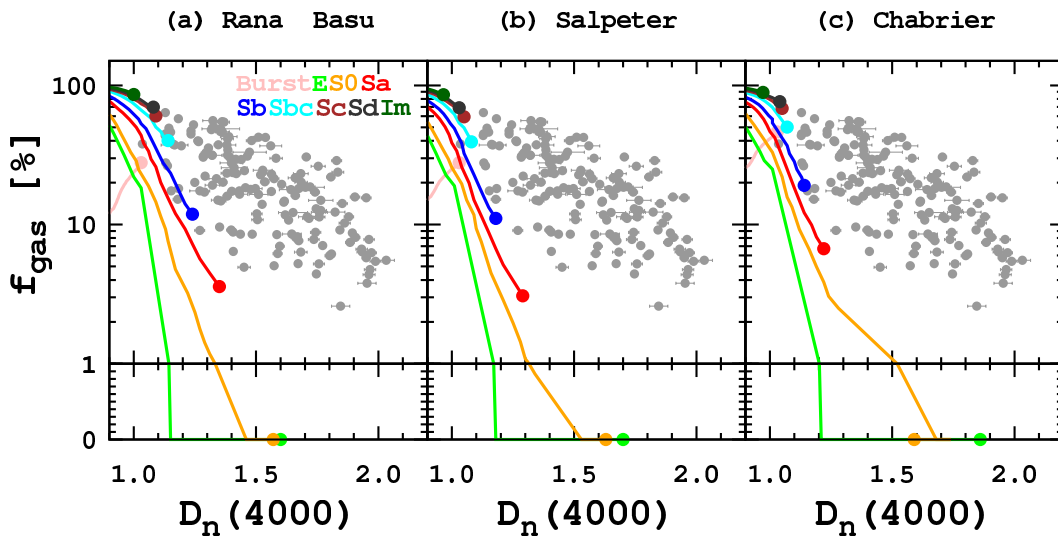


Fig. 8. Comparison between the observed $D_n(4000) - f_{\text{mol}}$ relation and the results of the PEGASE calculations in case of the IMF is (a) Rana & Basu (1992) (template scenario in PEGASE), (b) Salpeter (1955) and (c) Chabrier (2003). Filled circles represent COLD GASS galaxies from which both CO and HI emissions are detected (Cantinella et al. 2010; Saintonge et al. 2011). The color-coding of the lines are as follows: Burst in pink, E in light green, S0 in orange, Sa in red, Sb in blue, Sbc in light blue, Sc in brown, Sd in dark brown and Im in green. From $f_{\text{gas}} = 0$ to 1 %, the plot is in linear scale and from $f_{\text{gas}} = 1$ to 100 %, the plot is in log scale.

ent evolutionary scenarios (gas accretion and star-formation timescale) for different types of galaxies proposed in previous study based on optical SED, where later-type galaxies tend to have longer star-formation timescale normalized by total baryonic mass, and longer infall timescale, i.e., more recent gas accretion (Fioc & Rocca-Volmerange 1999). However there is a significant and qualitative difference between the observations and the model predictions, especially in $D_n(4000)$. Although the predicted gas fractions in spiral models (Sa \sim Sd) is almost consistent with the observed values, $D_n(4000)$ is too low compared to the observed values. In early-type galaxies (ETG) models, $D_n(4000)$ evolves to 1.6 but is still lower than the observed values (~ 1.9) for ETG in figure 8a.

4.1.1. Dependences on IMFs

We also calculated galaxy evolution with the same parameters except for the IMF. In the previous studies with PEGASE, Rana & Basu IMF (Rana & Basu 1992) was used to investigate the other parameters of galaxy evolution, such as star formation law and gas infall timescale, which reproduce observed optical spectra of each type of galaxy (Fioc & Rocca-Volmerange 1997; Fioc & Rocca-Volmerange 1999; Le Borgne & Rocca-Volmerange 2002; Tsalmantza et al. 2007). Figures 8b and c show the evolutionary path on the $D_n(4000) - f_{\text{gas}}$ plane in cases of two more widely used IMFs, Salpeter IMF (Salpeter 1955) and Chabrier IMF (Chabrier 2003), respectively. Although these two models also fail to reproduce the observed relation, there are slight but important differences among the three models. First, gas fractions of spiral models

at 13 Gyr with Chabrier IMF are larger than those with Salpeter and Rana & Basu IMFs. In addition, $D_n(4000)$ of ETG models at 13 Gyr with Chabrier IMF are larger than those with Salpeter and Rana & Basu IMFs. These results show that shape of IMF can change the $D_n(4000) - f_{\text{gas}}$ relation. We discuss how the choice of IMF changes the evolution of the $D_n(4000) - f_{\text{gas}}$ relation in the following paragraphs.

First of all, the difference in the shape of IMF changes the return gas mass from massive stars when they die. Compared to less massive stars, massive stars end their lives instantly from their births. Therefore, the IMF with a larger fraction of massive stars results in a larger gas fraction of galaxy at the time. The fraction of massive stars is larger in Chabrier IMF than Salpeter and Rana & Basu IMFs. This explains the difference seen in the gas fractions of spiral models at 13 Gyr among three models.

Chemical evolution is one of the important factors affecting $D_n(4000)$ evolution. Current galactic $D_n(4000)$ is determined by the gas phase metallicity when the major portion of stars were formed, and by the elapsed time since the major star-formation event occurred. It is because 4000 Å feature of galactic SED is formed by the metal absorptions of old stellar populations. Poggianti & Barbaro (1997) investigated the behavior of the 4000 Å index for a single star and for a single stellar population (SSP) as a function of age and metallicity. They explicitly showed that the strength of 4000 Å break becomes larger as the metallicity of star and SSP gets large. Different $D_n(4000)$ evolutions of galaxies according to metallicity were reported in Kauffmann et al. (2003) where a higher metallicity results in larger $D_n(4000)$ using population synthesis code of Bruzual & Charlot (2003). Kriek et al. (2011) reported a relation between $D_n(4000)$ and H α EW and showed that the observed relation is reproduced by the code of Bruzual & Charlot (2003) with a fixed metallicity of solar value through the evolution. Therefore, it is important to enlarge the metallicity of gas from which the stars are formed to increase $D_n(4000)$ of stars to the observed values.

The difference in the shape of IMF changes the chemical evolution. The gas released from the dead stars is metal enriched, thus the IMF with a larger fraction of massive stars results in earlier evolution of metallicity. Figure 9 shows the evolutions of gas phase and stellar metallicities with different IMFs. We can see that the model with Chabrier IMF has metal enriched at an earlier time. Gas phase and stellar metallicities of ETGs respectively become zero and almost constant (but gradually decreased with time) after the galactic wind blows out all the existing gas⁴. Thus, the ETGs model using the IMF with a larger fraction of massive stars results in larger $D_n(4000)$.

Higher metallicity of gas from which a major portion of stars is formed can increase $D_n(4000)$ as described above. However, at the same time, f_{gas} must go zero at the early epoch to increase $D_n(4000)$ in the existing condition. In

the next subsection, we discuss the possible reasons for the difficulty in reproducing the observed $D_n(4000) - f_{\text{gas}}$ relation quantitatively with the models.

4.2. Possible reasons for the discrepancy between observation and model calculation

In this section, we discuss possible reasons for the difficulty in reproducing the observed $D_n(4000) - f_{\text{gas}}$ relation in both sides of the model calculation and observation.

4.2.1. From the model-calculation side

One of the possibilities is the star-formation model in which stars are formed as long as gas exists regardless of the properties of gas component. According to the studies on star formation of the local universe, SFR is more closely related with dense molecular gas rather than total gas (e.g., Wong & Blitz 2002; Bigiel et al. 2008). Accreting gas is expected to be diffuse and with high temperature from cosmological simulation of galaxy evolution (Duffy et al. 2012). However, there is no model on transition from diffuse and hot gas to dense and cold gas in PEGASE. Once stars are newly formed, $D_n(4000)$ decreases because the luminosity-weighted SED becomes dominated by young and massive stars taking into account the mass-luminosity relation of main-sequence stars as $L \propto M^{3-4}$ (e.g., Popper 1980; Andersen 1991; Henry & McCarthy 1993). To increase $D_n(4000)$, it is necessary to form stars from metal-enriched gas and quench the star formation in the early time of the galaxy evolution. Therefore it is difficult to reproduce the galaxies with larger $D_n(4000)$ and non-zero gas fraction with the existing conditions in the model.

Morphological quenching (MQ) is an important process that can quench star formation even with a gas component, but which is not implemented in PEGASE. Martig et al. (2009) showed that once the central bulge becomes massive enough to stabilize the galactic disk against local gravitational instability, star-formation quenching occurs. Central concentration of ETGs leads to large epicyclic frequency κ , which is linked to the depth of the gravitational potential, and results in large Toomre's Q (Toomre 1964). As a result, the star formation in ETGs is quenched without a removal of gas component. We showed the concentration parameters of the COLD GASS sample in figure 7c. We can see that galaxies distributed in the lower-right corner in figure 7 mainly consist of ETGs. Therefore, our result suggests that they have large $D_n(4000)$ and non-zero gas fraction because MQ may work in those systems.

Re-accretion of the enriched gas in halo is also an important process for galaxy evolution especially in terms of chemical evolution, which is not modeled in PEGASE. Shen et al. (2012) investigated the metal-enriched circumgalactic medium (CGM) of a massive galaxy at $z = 3$ ($M_\star = 2.1 \times 10^{10} M_\odot$). They listed three sources of heavy elements in CGM in order of the fraction, 1) galactic wind from the main host, 2) "satellite progenitors" accreted by the main host before $z = 3$, 3) "nearby dwarfs" orbiting outside the virial radius. According to their result, the metallicity of accreting gas increases with time as a consequence of re-accretion of the metal-enriched gas in a "halo fountain" (Oppenheimer et al. 2010). Re-accretion

⁴ The gradual decrease of stellar metallicity in ETGs models in figure 9 is likely to be due to a small amount of accretion of metal-zero gas.

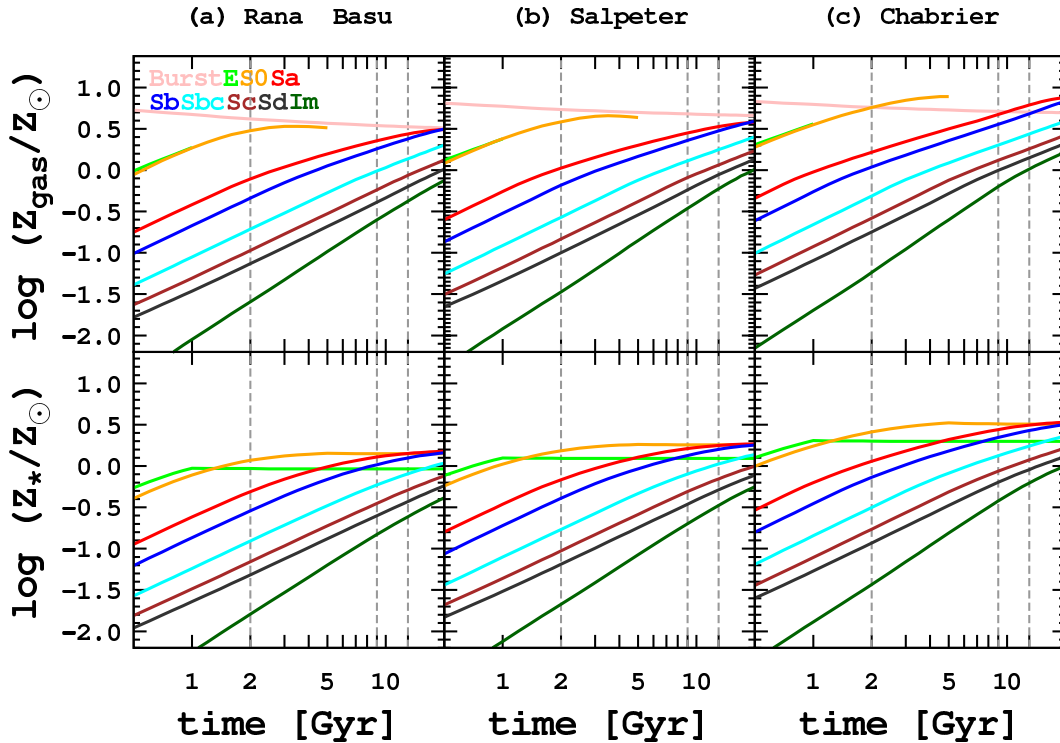


Fig. 9. Evolution of gas phase (upper panels) and stellar metallicities (lower panels) normalized by the solar value ($Z_{\odot} = 0.0134$, Asplund et al. 2009). The dashed lines indicate the 2, 9 and 13 Gyrs, which are the ages of each type of galaxy specified in table 3. The color-coding is the same as figure 8.

of the enriched gas is likely to promote chemical evolution and increase $D_n(4000)$ of modeled spiral galaxies. In addition, since re-accretion is reported to be more promoted in more massive systems due to the deceleration by the interaction with dense halo gas (Oppenheimer & Dave 2008; Oppenheimer et al. 2010), the larger discrepancy in $D_n(4000)$ of more massive galaxies may be compensated.

4.2.2. From the observation side

The results of PEGASE calculation is a galactic $D_n(4000) - f_{\text{gas}}$ relation since PEGASE assumes a galaxy as an one-zone system. However, the gas mass of galaxies used in this study is a total mass and $D_n(4000)$ is calculated using data obtained within the SDSS 3-arcsec fiber. Therefore it is not clear whether the obtained $D_n(4000) - f_{\text{gas}}$ relation is a relation between galactic star formation history and galactic gas fraction or star-formation history of central bulge and galactic gas fraction. Therefore, the much larger $D_n(4000)$ obtained with the observation than those in model prediction may be partly attributed to this situation, since most galaxies have metallicity gradients (e.g., Sanchez et al. 2014). Considering that most disk galaxies have exponential profile of molecular gas distribution and most ETGs have molecular gas distribution with a relatively small extent (e.g., Davis et al. 2013; Alatalo et al. 2013), the contribution of CO emission from central part to the total CO flux is large in both cases. Thus it may be a relation indicating the evolution of central bulge. To understand the physical background of this relation, it is important to compare spatially disaggregated $D_n(4000)$ and gas fraction.

The universality of this relation should be investigated with higher- z galaxies. Recent CO observations towards galaxies at $z = 1 - 2$ revealed extremely high molecular gas fractions ($\sim 50\%$) in those systems (e.g., Tacconi et al. 2013). The measurement of $D_n(4000)$ of those systems allows us to enlarge the f_{mol} as well as the redshift ranges at the same time. Although the reported $D_n(4000) - f_{\text{mol}}$ relation in this study has already given the important suggestion, once the observational assessments for the tasks described above are completed, this relation would be one of the strict observational constraints on the models for galaxy formation and evolution.

5. Summary

We observed 12 normal galaxies at $z \sim 0.1 - 0.2$ with the 45-m telescope at NRO to measure the molecular gas mass and investigate the relation between star formation history and molecular gas fraction f_{mol} . The sample galaxies are selected with $D_n(4000)$ instead of the widely used FIR flux. The main results obtained in this paper are as follows:

1. We detect the CO emissions from six galaxies with $S/N > 4$, two galaxies with $3 < S/N < 4$ out of 12 samples and show the validity of the sample selection based on $D_n(4000)$.
2. Using the literature data of nearby galaxies (Saintonge et al. 2011), we find a tight anti-correlation between $D_n(4000)$ and f_{mol} indicating

that more gas-rich galaxies tend to have younger stellar populations than gas-poor galaxies for the first time.

3. We show that our sample galaxies at $z \sim 0.1 - 0.2$ follow the same $D_n(4000)$ relation of the nearby galaxies. This suggests that galaxies might evolve along this relation and that $D_n(4000)$ might be used as proxy for f_{mol} which requires much telescope time to be measured.
4. We calculate the galaxy evolution with a population synthesis code PEGASE (Fioc & Rocca-Volmerange 1997) to investigate the observed $D_n(4000) - f_{\text{gas}}$ relation. We calculate the total gas fraction f_{gas} with literature data of nearby galaxies and compare with the model calculations. As a result, any template scenarios for different morphological types, which have been constructed so as to reproduce optical SED, cannot reproduce the observed relation.
5. Our results suggest that star formation from metal enriched gas and star formation quenching in the early time are necessary to form galaxies with the observed large $D_n(4000)$ and non-zero gas fraction.

We would like to thank an anonymous referee for very productive comments. KMM thanks Kouji Ohta, Tadayuki Kodama, Takashi Okamoto, Yoichi Tamura, Shinya Komugi, Nick Scoville, Tomoki Morokuma and all members of NRO for their support and fruitful discussions.

PEGASE calculations were carried out on computers at the Center for Computational Astrophysics, National Astronomical Observatory of Japan. JB was supported by HPCI Strategic Program Field 5 “The origin of matter and the universe” and JSPS Grant-in-Aid for Young Scientists (B) Grand Number 26800099.

Funding for SDSS-III has been provided by the Alfred P. Sloan Foundation, the Participating Institutions, the National Science Foundation, and the U.S. Department of Energy Office of Science. The SDSS-III web site is <http://www.sdss3.org/>. SDSS-III is managed by the Astrophysical Research Consortium for the Participating Institutions of the SDSS-III Collaboration including the University of Arizona, the Brazilian Participation Group, Brookhaven National Laboratory, Carnegie Mellon University, University of Florida, the French Participation Group, the German Participation Group, Harvard University, the Instituto de Astrofísica de Canarias, the Michigan State/Notre Dame/JINA Participation Group, Johns Hopkins University, Lawrence Berkeley National Laboratory, Max Planck Institute for Astrophysics, Max Planck Institute for Extraterrestrial Physics, New Mexico State University, New York University, Ohio State University, Pennsylvania State University, University of Portsmouth, Princeton University, the Spanish Participation Group, University of Tokyo, University of Utah, Vanderbilt University, University of Virginia, University of Washington, and Yale University.

References

- Ahn, C. P., et al., 2012, *ApJS*, 203, 21
Ahn, C. P., et al., 2014, *ApJS*, 211, 17
Alatalo K. et al., 2013, *MNRAS*, 432, 1796
Andersen, J., 1991, *A&ARv*, 3, 91
Asplund, M., et al., 2009, *ARA&A*, 47, 481
Baldwin, J. A., et al., 1981, *PASP*, 93, 5
Balogh, M. L., et al., 1999, *ApJ*, 527, 54
Bauermeister, A., et al., 2013, *ApJ*, 768, 132
Bigiel F., et al., 2008, *AJ*, 136, 2846
Bolatto A. D. et al., 2013, *ARA&A*, 51, 207
Brinchmann, J., et al., 2004, *MNRAS*, 351, 1151
Bruzual, G., & Charlot, S., 2003, *MNRAS*, 344, 1000
Cantinella B. et al., 2010, *MNRAS*, 403, 683
Chabrier, G., 2003, *PASP*, 115, 763
Chang R. X. et al., 2010, *ApJ*, 722, 380
Chung A. et al., 2009, *AJ*, 138, 858
Combes, F., et al., 2013, *A&A*, 550, 41
Conselice, C. J., 2006, *MNRAS*, 373, 1389
Davis, T. A. et al., 2013, *MNRAS*, 429, 555
Duffy et al., 2012, *MNRAS*, 420, 2799
Fioc, M. & Rocca-Volmerange, B., 1997, *A&A*, 326, 950
Fioc, M. & Rocca-Volmerange, B., 1999, *A&A*, 351, 869
Geach, J. E., et al., 2011, *ApJ*, 730, 19
Henry & McCarthy, 1993, *AJ*, 106, 773
Kauffmann, G., et al., 2003, *MNRAS*, 341, 33
Kauffmann, G., et al., 2012, *MNRAS*, 422, 997
Kennicutt, R. C. & Evans, N. J., 2012, *ARA&A*, 50, 531
Kriek, M. et al., 2011, *ApJ*, 742, 168
Le Borgne, D. & Rocca-Volmerange B., 2002, *A&A*, 386, 446
Leitner, S. N., 2012, *ApJ*, 745, 149
Lilly, S. J. et al., 2013, *ApJ*, 772, 119
Martig M. et al., 2009, *ApJ*, 707, 250
Matsui, K., et al., 2012, *PASJ*, 64, 55
Nakajima, T., et al., 2013, *PASP*, 125, 252
Oppenheimer B. D. & Dave R., 2008, *MNRAS*, 387, 577
Oppenheimer, B. D., 2010, 2010, *MNRAS*, 406, 2325
Petrosian, V., *ApJ*, 209, 1, (1976)
Poggianti, B. M. & Barbaro G., 1997, *A&A*, 325, 1025
Popper, D. M., 1980, *ARA&A*, 18, 115
Rana, N. C. & Basu S., 1992, *A&A*, 265, 499
Saintonge, A. et al., 2011, *MNRAS*, 415, 32
Salpeter, E. E. 1955, *ApJ*, 121, 161
Sanchez, S. F., et al. 2014, *A&A*, 563, 49
Sanders, D. B., et al. 1988, *ApJ*, 325, 74
Sanders, D. B., & Mirabel, I. F. 1996, *ARA&A*, 34, 749
Shen, S., et al., 2012, *ApJ*, 760, 50
Shimasaku K. et al., 2001, *AJ*, 122, 1238
Solomon P. M. et al., 1997, *ApJ*, 478, 144
Strateva, I. et al., 2001, *ApJ*, 122, 1861
Tacconi, L. J., et al., 2013, *ApJ*, 768, 74
Toomre A., 1964, *ApJ*, 139, 1217
Tremonti, C. A., et al., 2004, *ApJ*, 613, 898
Tsalmantza, P. et al., 2007, *A&A*, 470, 761
van Dokkum, P. G., et al., 2013, *ApJL*, 771, 35
Wong T. & Blitz L., 2002, *ApJ*, 569, 157
Woosley S. E. & Weaver T. A., 1995, *ApJS*, 101, 181